An Experimental Study of the Near Wake of Horizontal Axis Wind Turbines

Mina G. Mourad, Samir S. Ayad, Osama E. Abdellatif and Ali A. Abdelaziz

Shoubra Faculty of Engineering, Benha University

108 Shoubra St., Cairo 11511, Egypt

Corresponding Author: samir_ayad@mail.com

Abstract

The present work considers an experimental investigation of wind turbine near wake by using Particle Image Velocimetry (PIV) visualization technique. The PIV technique gives a complete picture of all points at the domain under consideration. The study is focused on the effect of tip speed ratio (λ) and Reynolds number (Re_c) on the near wake characteristics. A three-blade model of wind turbine with airfoil SG 6040 16% is tested in water channel at Re_c range between 1.28×10^4 and 7.68×10^4. Various tip speed ratios are tested between $\lambda=2$ and $\lambda=12$. Experiments are also performed at constant $\lambda=8$ and variable Re_c in the range between 2.56×10^4 and 5.12×10^4.

The results show that as λ increases both wake width and length increase up to $\lambda=9$. For higher values of l, the wake width remains constant. The turbulence intensity measurements show that an increase of λ causes an increase of turbulence intensity in the wake. Experiments at constant tip speed ratio $\lambda = 8$ and variable Reynolds number showed smaller values of turbulence intensities, narrower and shorter wakes at lower values of Reynolds number. The tip vortices pitch showed its dependence on the number of blades (B) and tip speed ratio (λ). The pitch is weakly affected by Re_c increase.

The wake rotation study showed significant effects on inflow angle (ϕ) and power coefficient especially at low tip speed ratio.

1. Introduction

Due to the increasing demand for wind energy, extensive research is being done to support wind turbine design. Current industry codes for calculating wind turbines rotor loads and power output are based on blade element momentum theory (BEMT) [1]. BEMT contains fundamentally invalid assumptions [2], which are overcome in practice by empirical adjustments.

Wind turbine wake is one of the most important regions must be studied for better understanding of the aerodynamics behavior. The wake can be divided into two regions: near wake region and far wake region. The near-wake region is the region immediately behind the rotor. At the near wake, the presence of the turbine blades is most prominent and the flow field is three dimensional [3]. The extent of the near wake region can be approximated as one diameter downstream from the rotor plane. The far wake is important to the mutual dependence of wind turbines in a wind farm and the issue of positioning them to ensure maximum efficiency in wind farm operations [4].

An experiment was conducted to investigate the near-wake formation and development to provide datasets for validation of near-wake calculation models [5]. Three-dimensional velocity fields were measured by hot wire anemometry at different azimuthal blade positions using phase-locked averaging. The authors reported azimuthal variation of velocity vectors at the rotor plane

and extracted the value of axial induction factor at the rotor plane. The results were useful for BEMT improvement as BEMT relies heavily on the values of induction factor at the rotor plane.

Formation, development and properties of the near wake were investigated experimentally by hot-wire anemometry over different tip speed ratios [6]. The authors found the distribution of circumferentially averaged velocity deficit and mean velocity.

The hot wire anemometry limitations in measurements are the reasons which made authors directed to Particle image velocimetry (PIV). Quantitative flow visualization techniques like PIV have been very popular in the area of experimental fluid dynamics due to their non-intrusive characteristic and the fact that very rich flow information can be obtained. PIV can give information very near to the rotor plane or even at the rotor plane to investigate the influence of the rotor on the flow field around it [4].

Bound circulation and tip vortex detailed profiles were presented for the first time by using PIV [7]. The authors successfully identified the application of PIV as a tool for measuring velocities around wind turbine model.

PIV measurements were taken downstream of a horizontal axis wind turbine model in a water channel to compare the results with full-scale measurements [8]. The wake velocity deficits of model-scale and full-scale measurements had significant differences. These differences were suggested to be due to scaling effects, blockage effects and uncertainties associated with the full-scale experiment.

Velocity and vorticity of the near wake are studied for validation of the inviscid free-wake code, Rotor Vortex Lattice Method (ROVLM), developed in the University of Stuttgart [1]. The ROVLM results agreed with the experimental results qualitatively as it predicted the shape of the wake boundary and the contraction of the wake in the downstream side very well. The code failed to predict the influences of Reynolds number.

To study the flow structure in the wake of the wind turbine, database of the initiation and development of the tip vortex was required. A large-view flow field measurements using the PIV technique with high resolution CCD cameras are performed [9]. The results showed that the tip vortex first moved inward for a very short period and then moved outward with the wake expansion. The measurements also indicated that the downstream movement of the tip vortex was nearly linear in the very near wake under the test condition.

Dynamic wind loads and the evolution of the wake vortex and turbulent flow structures in the downstream of a horizontal axis wind turbine are studied [10]. The characteristics of the turbulent wake flow including the evolution of the helical tip vortices, velocity deficits, and turbulent properties were found to vary significantly as a function of the tip speed ratio of the wind turbine.

The vortical near wake of a model horizontal axis wind turbine was investigated experimentally in a water channel to study vortex interaction and stability of the helical vortex filaments within a horizontal axis wind turbine wake [11]. The helicoidal pitch reduced with increasing tip speed ratio causing the wake to become unstable closer to the rotor plane. The authors suggested to consider airfoil performance during the design of low Reynolds number rotary or fixed-wing experiments.

Tip speed ratio is the most studied parameters to show its effect on tip vortices and velocity deficit in the wake. The effect of Reynolds number variation on the wake expansion is not covered well. So, Reynolds number effect on the initial wake expansion and on the thrust coefficient in scaled wind turbine tests was studied [12]. It was found that wake width and expansion became narrower by decreasing Re_c. It was also observed that the tip vortex pitch was not strongly affected by Reynolds number.

The previous studies focused on the tip vortices growth downstream the wake and stream-wise velocity deficit by several measurement devices. It also showed the importance of

studying the near wake in order to show its effect on the rotor performance. Wake rotation effect on the rotor performance was not clear in most of the previous research work. Axial induction factors, as well as the tangential induction factors, were evaluated only at blade tip.

The present study focuses on wake rotation effect on the rotor performance and airfoil characteristics. The study aims to find the correlation between the tip vortices pitch and the induced velocities behind the rotor. Since most of the previous studies were performed at low turbulence intensities, the present study is performed at higher turbulence level to show its effect on tip vortices intensities. The effect of Reynolds number on the tip vortices pitch, vortex intensity, velocity deficit, wake expansion and turbulent intensity will be also studied at constant tip speed ratio. Based on PIV measurements the axial induction factor as well as the tangential induction factor will be calculated at all radial positions of the rotor in order to evaluate the effectiveness of the different radial sections of the blade and to enable new designs to enhance the produced power.

2. Experimental Procedures

2.1.   Wind turbine model

A three-blade model of wind turbine is fabricated by 3D printing machine (EOS 3D Printer) of The Central Metallurgical Research and Development Institute (CMRDI) at Tabbin. The used model design is used before in a previous research [13], but it is modified to be three-bladed model. The model diameter is 74 mm with Selig/ Giguere SG 6040 wind turbine airfoil.
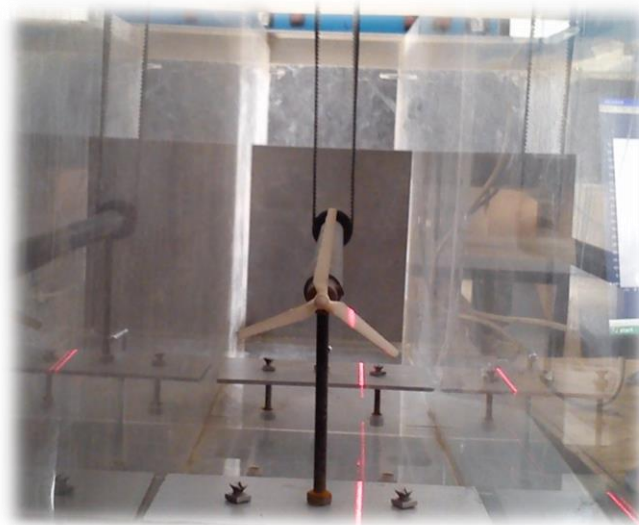
Fig. 1*: A picture of the 3-blade model fixation in water channel*

The chosen airfoil (SG 6040 16%) is classified as a low Reynolds number airfoil that is appropriate for the range of Reynolds number used in the present experiment.
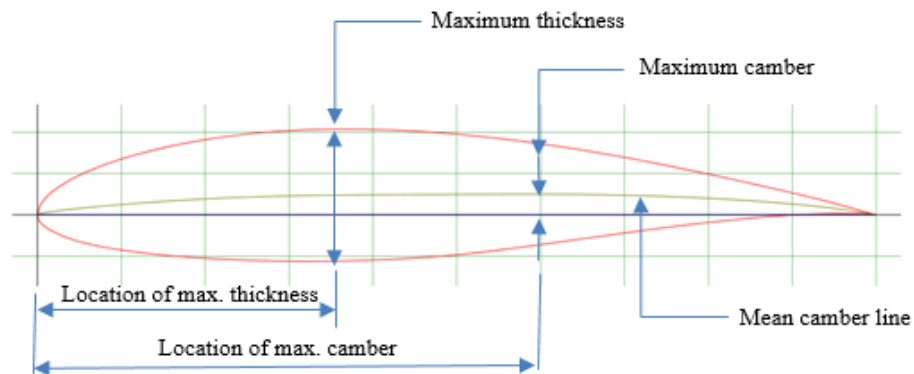
Fig. 2: *Schematic diagram of SG 6040 airfoil*

2.2. Water channel preparation

Hydraulic demonstration channel of Engineering laboratory Design (ELD) is used to demonstrate flow through it. The ELD working channel is existing in hydraulic laboratory of Shoubra faculty of Engineering with dimensions 0.15 m wide by 0.3 m deep by 2.43 m long.

Fig. 3: *A picture of PIV system setup and its connection to computer*

Direct current (DC) motor is used to drive the turbine model and the power is transmitted from the motor to the rotor shaft by using a toothed belt. The motor rotational speed is controlled by using Pulse Width Modulation (PWM) electrical circuit. Laser tachometer are used in order to adjust the required rotor speed.
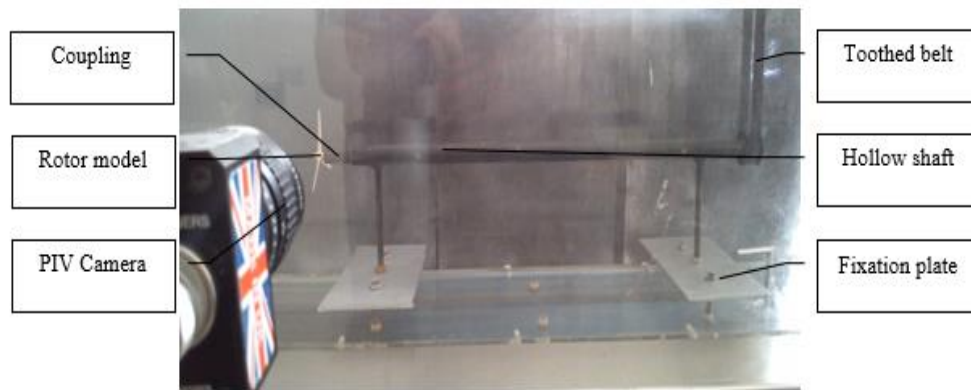
Fig. 4: *A picture of model rotor supporter and its components*

2.3.   Particle image velocimetry

The particles are tracked by taking 2 photographs a short period (Δt) apart. The flow is illuminated using the thin sheet of laser light (3 mm). The pair of photographs is often referred to as Frame A and Frame B, and it is important that these two images show instantaneous "snapshots" of the particles positions.
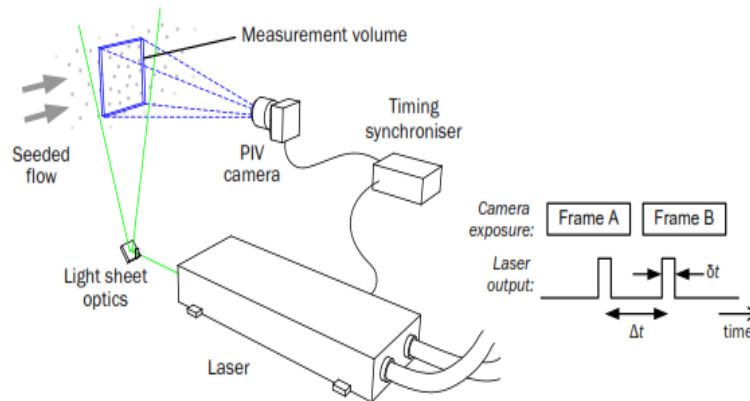
Fig. 5: *Schematic diagram of the PIV system setup and time synchronizing*

2.3.1. Multi-pass correlation

This can be useful for flows that contain small scale features, where the first pass might be too large to reliably represent the flow. For experiments that contain both fast and slow areas of flow however, such small Δt values can significantly decrease the measurement's signal-to-noise ratio, within the slow areas.

2.3.2. Seeding particles

The present study uses Polyamide powder seeding particles of 50 μm diameter and about 999 kg/m³ density. Seeding particles must be with suitable diameter in order to reflect light. Seeding particles density must be close to the water density in order to avoid particles slipping.

3. Results and discussions

Various Tip Speed Ratios (λ) between 2 and 12 are used with flow velocity 0.16 m/s and Reynolds number (based on the chord length and tip speed velocity) (Re_c) between 1.28×10^4 and 7.68×10^4. To investigate the effect of Re_c separately, experiments are carried out with same value of tip speed ratio ($\lambda=8$), while Re_c varies from 2.56×10^4 to 5.12×10^4. Time-averaged velocity maps, tip vortices properties and turbulent intensity maps are extracted by PIV software. All measurements are extracted at a 0.2 R offset from the rotor centerline to avoid the interference of the laser light sheet and the rotor hollow shaft.

3.1.   Time averaged velocity variation with λ

Stream-wise velocity maps are extracted by using 64 pixels initial pass, 8 pixels final window size and 50% overlapping.
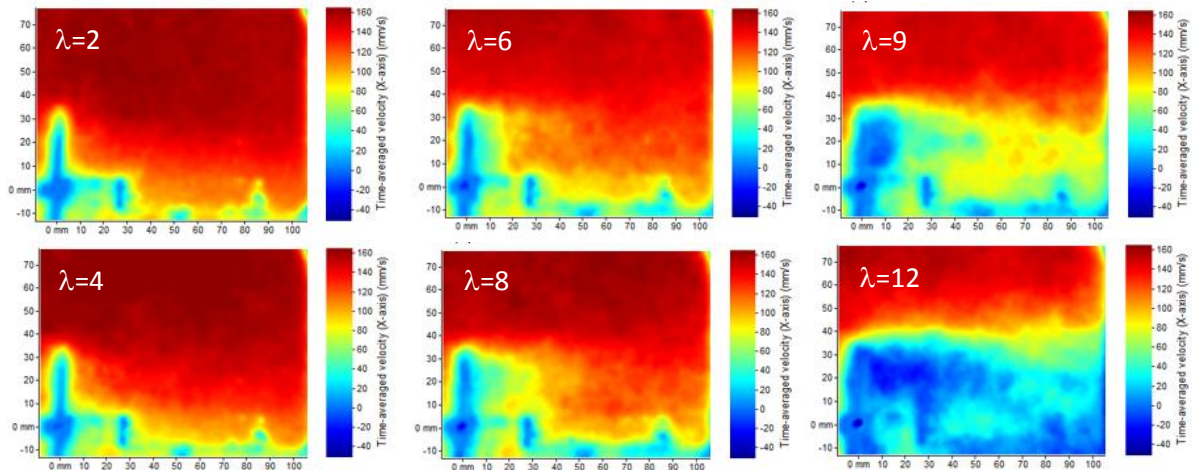
Fig. 6: *Stream-wise velocity maps at different values of λ and Re_c*

The previous figures of the stream-wise velocity maps describe the wake boundary and shape of the near wake behind the turbine model. The present study has considered 0.85 U∞ is the maximum limit for the wake boundary as shown by **Fig. 7**. It is pronounced that the wake width and length is a function of λ. At $\lambda=2$ the wake width and length are limited to about 0.8 R and 0.7 R respectively. As the tip speed ratio increases the wake is further extended downstream and wake width increases to reach turbine radius (R) at $\lambda \geq 9$ and the wake occupies the entire studied region X/R=2.7.

The wake outer boundary which separates the free-stream and mixing region is shown by **Fig. 7** at the studied range of λ. The mixing layer is more pronounced at stream-wise flow maps

from λ=6 to λ=12 by the region which is trailed from the rotor tip and diverged downstream the wake. Maps for $\lambda \geq 9$ show reverse flow close to the rotor which is also supported by the momentum theory [14]. Reverse flow is the main reason of power loss since it reduces the pressure difference across the rotor.
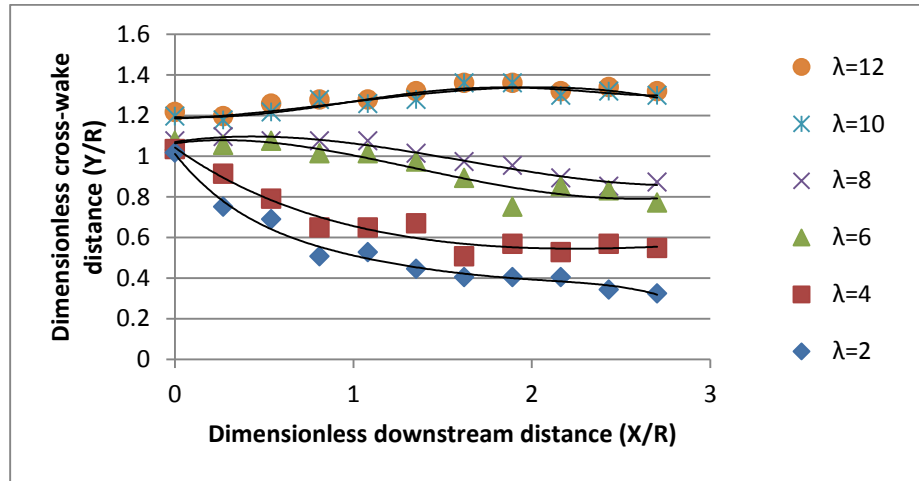
Fig. 7: *Wake width variation downstream the rotor at various λ and Re_c*

The figure verifies what was explained about wake expansion and wake width. There aren't any changes about wake width at $\lambda \geq 10$ thus; rotor acts as a solid disc with the same diameter at $\lambda \geq 10$.

3.2.   Time averaged velocity variation with Re_c

For the same free-stream velocity as λ increases the Reynolds number also increases. To investigate the effect of Re_c, free-stream velocity should be varied with the rotor speed variation. The following figures are averaged velocity maps at constant λ (λ=8).
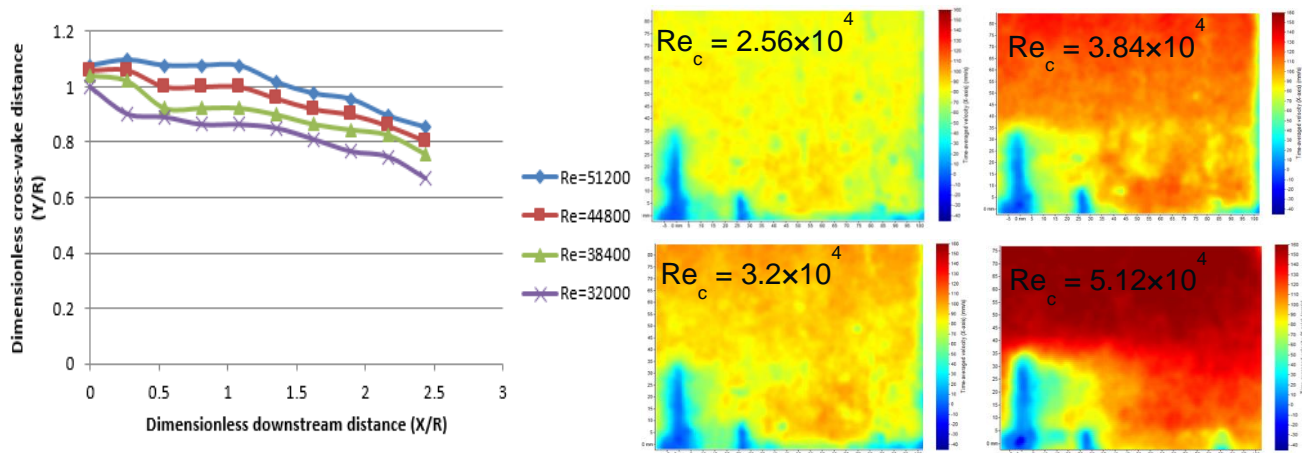
Fig. 8: *Stream-wise velocity maps at different values of Re_c*

7

The velocity maps in *Fig. 8* show that as Re_c increase the wake width and expansion increase. Reynolds number has a significant effect on velocity deficit behind the rotor. The velocity deficit results which are obtained before from λ variation must include Re_c effect.

3.3.   Turbulence intensity variation with λ

Turbulent intensity (TI %) is very important parameter in wind turbine wake study. Turbulence intensity is used as a measure of fatigue loads on various components of the turbine [15]. The free-stream turbulence intensity (TI %) is about 25%. High value of turbulence intensity is used in order to show the effect of turbulence intensity on tip vortices intensity.
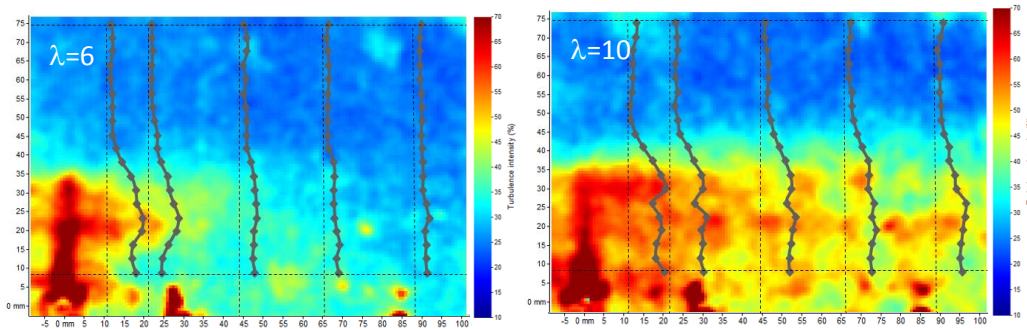
Fig. 9: *Turbulence intensity distribution map at different values of λ and Re_c*

Fig. 9 shows that turbulent intensity increase by increasing λ. It is concentrated at the region immediately behind the rotor especially at the highest λ values. It is clear that there are high turbulence at Y/R=0.6 and extends downstream the wake. Flow separation at the leading edge of the airfoil at low Reynolds number range is the reason TI increase with λ. Leading edge separation is most likely to occur while operating at Re_c range between 10^4 and 10^5 [16].

3.4.   Turbulence intensity variation with Re_c

The previous extracted maps of turbulence intensity at various tip speed ratios include Reynolds number variation effect. The same experiments are carried out for various flow and rotor speeds at constant λ=8 in order to demonstrate Re_c effect as follows.
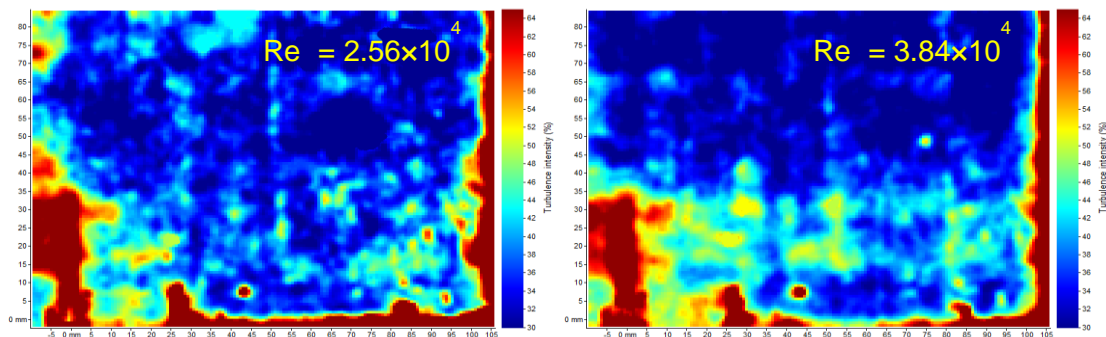
Fig. 10: *Turbulence intensity distribution maps at different values of Re_c at constant λ (λ =8)*

Fig. 10 show that turbulence intensity is affected by Re_c variation. Turbulence intensity increases as Re_c increase at constant λ. Turbulence intensity maps of λ variation (*Fig. 9*) must contain Re_c effect.

3.5.   Tip vortices pitch and intensity variation with λ

Tip vortex is formed by the effect of the pressure difference between the lower and upper side of blade. The tip vortices are trailed from blades tips and rolls up in a helical path which rotates in an opposite direction of rotor rotation. The pitch (h) is defined as the mean axial distance between the tip vortices centers. It is measured for different values of the tip speed ratio λ from 2 and 12. The vortices maps are extracted by using 32 pixels initial pass, 12 pixels final window size and 50% overlapping. Such conditions are suitable for the considered range of λ and present resolution of the camera.
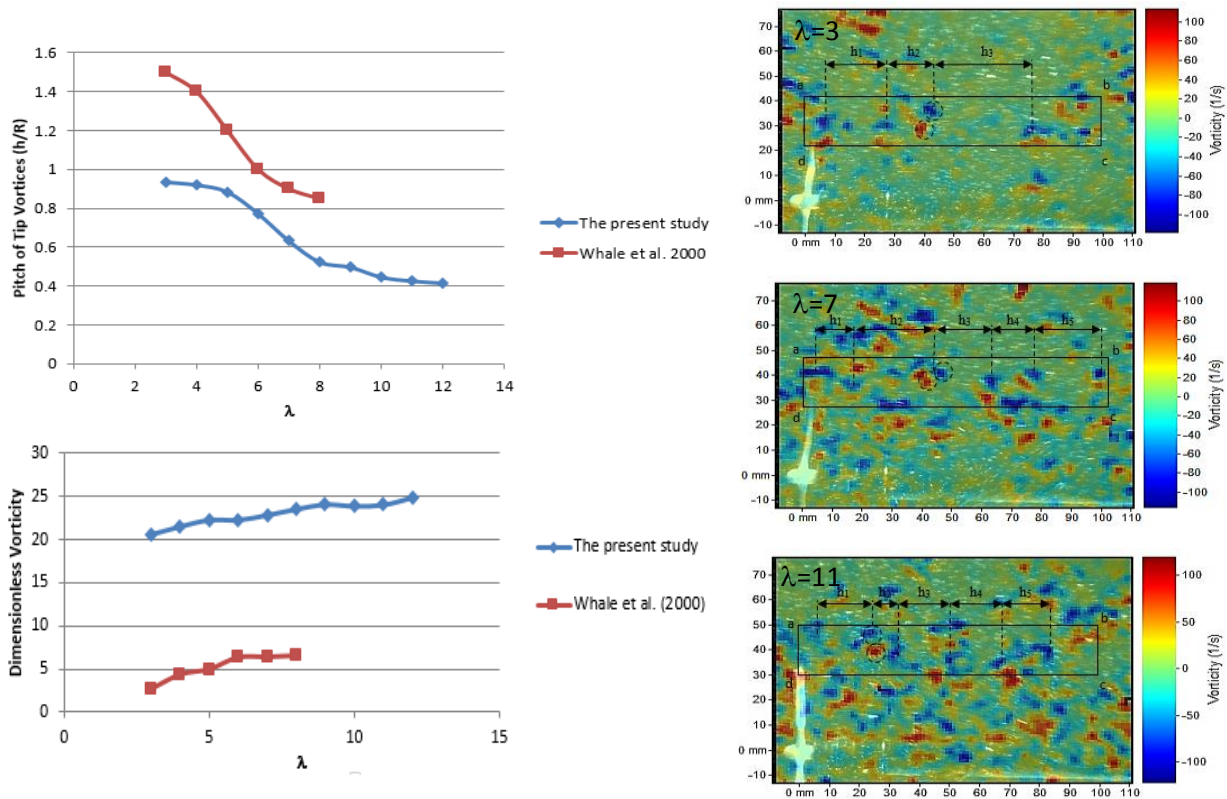
Fig. 11: *Tip vortices distribution maps at different values of λ and Re_c*

Tip vortices are considered the limit of wake boundary but they don't take the same positions of wake width which are presented in *Fig. 7*. Wake meandering is the reason for that since it is a term used for the large scale movement of the entire wake [17]. *Fig. 11* shows that the dimensionless pitch (h/R) values decrease by increasing λ. The comparison between the present results and those of the authors [1] show a difference for each corresponding λ. These differences are due to use of three-blade model in the present study. The authors [1] have used two-blade flat model.

The comparison between dimensionless tip vortices vorticity (ϖ) (1) of the present study and those of the authors [1] shows the same trend, i.e. that vorticity increases as λ increases. The comparison shows also a constant difference between tip vortices intensities at each point since tip vortices of the present study are about 7.5 times those of the authors. The high turbulence intensity of the present study is the reason of the difference since the used turbulent intensity is about 6.25 times those of the authors [1].

$$\varpi = \frac{\omega R}{U_\infty} \tag{1}$$

3.6.   Tip vortices pitch and intensity variation with Re_c

The Reynolds number effect on tip vortices were not clear in the previous vortices maps since, they contain the effect of λ and Re_c together. Tip vortices maps are extracted at constant λ (λ=8) and Re_c range between 2.56×10^4 and 5.12×10^4.
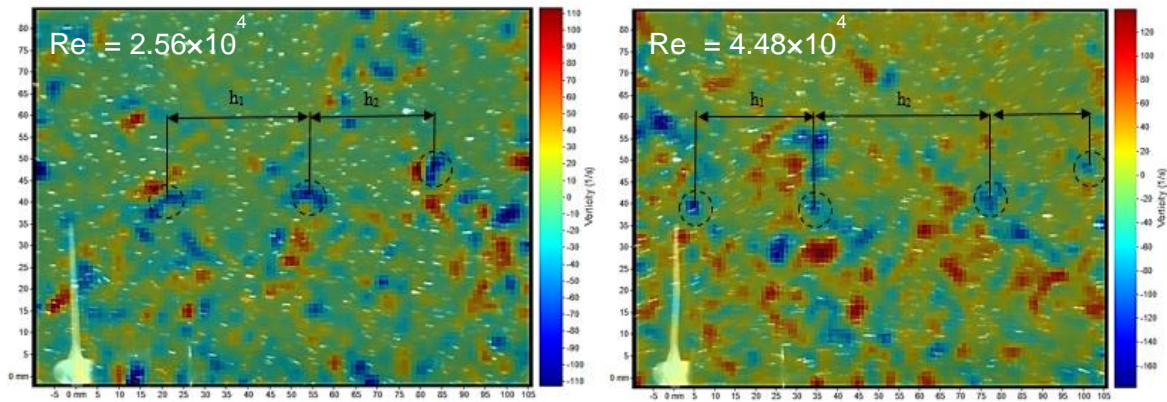
Fig. 12: *Tip vortices distribution maps at different values of Re_c and constant λ*

The tip vortices variation with Re_c shows that the tip vortices pitch was not strongly affected by Re_c and that confirms a performed results in the literature [12]. Tip vortices intensity have a slight increase as Re_c increases because of the turbulence intensity increase.

4. Performance prediction using the measured parameters

4.1.   Axial and tangential induction factors

Axial and tangential induction factors (a) and (a') respectively are important parameters in wind turbine rotor design. Blade Element Momentum Theory (BEM) theory suggests steps to obtain a and a' by iterations to get the final design of blade dimensions, twist angle and pitch angle (β).

The present study results provides the extracted stream-wise velocity data downstream the rotor at X/R=0.32 as discussed before. Axial induction factor (a) variation with the radial

10

position from the rotor axis is calculated by the wake velocity at the mentioned position. The axial induction factor is calculated according to Eq. (2).

$$a = \frac{(U_\infty - U_w)}{2U_\infty}$$

(2)
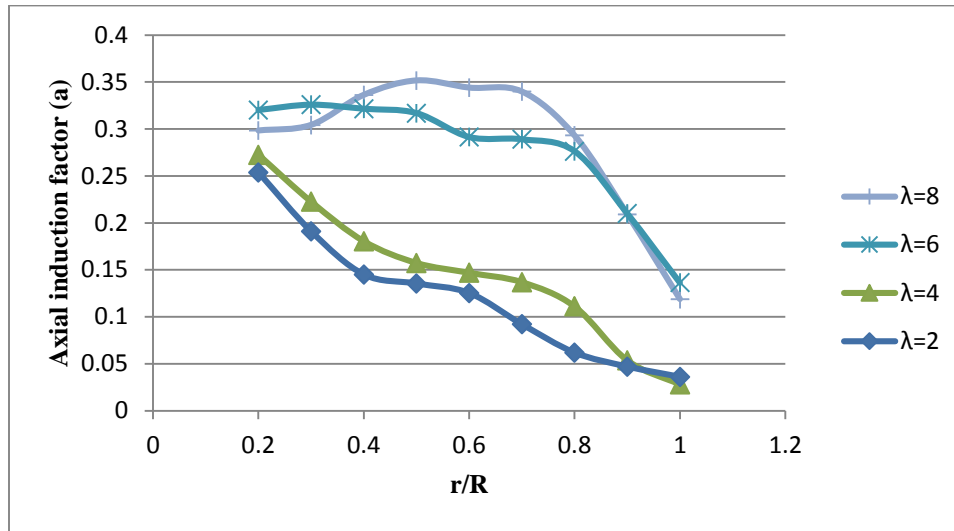
Fig. 13: *Variation of axial induction factor with radial position at different values of λ*

Fig. 13 shows that the axial induction factor decreases gradually as radial position increases (closeness to the tip) at low values of λ from λ=2 to λ=4. At high values of λ, the axial induction factor curves take another trend. For 6 ≤ λ ≤ 8, the induction factor stay almost constant up to r/R=0.8 and then decreases with radius. It is important to notice that, for this range, the value of axial induction factor is very close to the optimum value based on Betz limit (a=0.3). That confirms the most common usage of λ range between 6 and 8.

The tip vortices intensity of the helical path plays an important role to form the root vortex. The root vortex is firstly responsible for inducing the tangential velocity in the wake flow [14]. The root vortex has circulation (Γ) which obtained from the tip vortex circulation (ΔΓ) by using Eq. (3) [17].

$$\Gamma = B\Delta\Gamma$$

(3)

The tangential induction factor (a') is calculated at each radial position of the rotor by using Eq. (4).

$$a' = \frac{\Gamma}{4\pi r^2 \Omega} \tag{4}$$
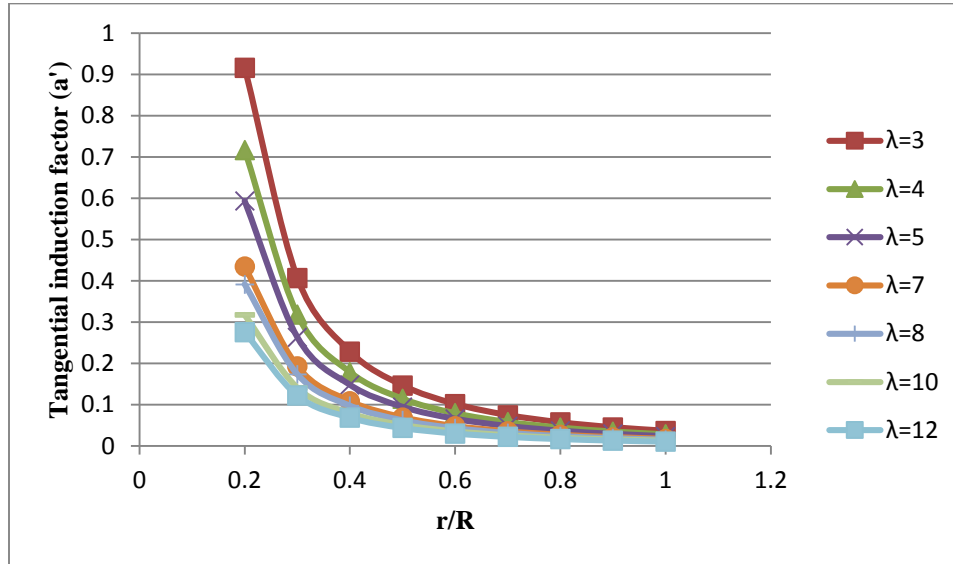
Fig. 14: Variation of tangential induction factor against radial position at different values of λ

The tangential induction factor (a') values become lower by increasing λ as demonstrated by **Fig. 14** which reflects that the effect of wake rotation is reduced by increasing λ. This observation will be pronounced in inflow angle (ϕ) distribution and power coefficient (C_p).

4.2.   Inflow angle

Calculations of inflow angle (ϕ) are needed to determine the suitable pitch angle (β) for each section of the used blade. Twist angle for each blade can be easily determined by knowing (β) in order to adjust each section to make suitable angle of attack (α) for higher C_L/C_d ratio. Inflow angle (ϕ) is calculated taking the effect of tangential induction factor (a') into consideration as:

$$\tan \phi = \frac{U_\infty (1 - a)}{\Omega r (1 + a')} \tag{5}$$

Inflow angle can be also calculated using the mean value of tip vortices pitch (h) and the rotor radius (R) by using Eq. (6) [11]. The value of inflow angle from Eq. (6) is considered at the tip of the rotor. A comparison is performed for the ϕ values from Eq. (5) and Eq. (6) at the tip.

$$\tan \phi = \frac{h}{2\pi R} \tag{6}$$
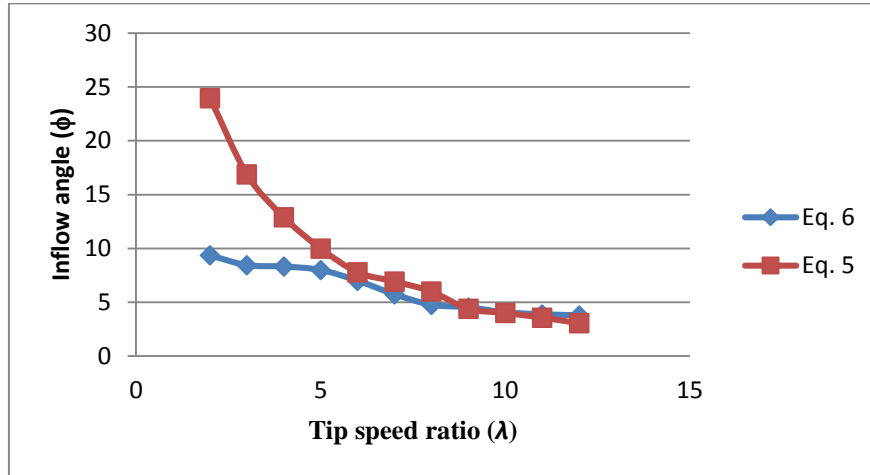
Fig. 15: Comparison between inflow angles based on induction factors at the tip and those on tip vortices pitch

The comparison demonstrated by **Fig. 15** shows a good agreement of inflow angle values starts from $\lambda=5$ up to $\lambda=12$. The observed deviation at low values of λ is due to the use of constant value of r=R. At small tip speed ratios range, the helical path radius (r) of the vortices decreases downstream the wake as shown by the velocity scalar maps. The helical path radius becomes constant and equal to the rotor radius approximately at high tip speed ratios range. Taking a constant radius (R) for all the range of λ causes a deviation in the results, especially at low λ range. The comparison confirms that PIV measurements give good estimation for induction factors as well as for the vortices pitch, especially at the higher values of tip speed ratio.

4.3.   Power coefficient

Power coefficient is calculated by using the axial induction factor (a) from Eq. (7) which is obtained at each element of the rotor blade.

$$C_p = 4a(1-a)^2 \tag{7}$$

The local values of C_p at the blade elements are calculated for each λ to present the mean value C_p for each λ. There are two equations to calculate local C_p, Eq. (7) doesn't take wake rotation into account while Eq. (8) [18] takes wake rotation into account. The first term of the equation is based on One-dimensional momentum theory, while the second term accounts for the power loss due to the wake rotation calculated for a cylindrical wake with a constant circulation on the blade.

$$C_p = 4a(1-a)^2 - [(1-a)(\frac{v_R}{U_\infty})^2] \qquad \textbf{(8)}$$

The authors [18] has defined (v_R) as the velocity vector in the rotating system which is obtained from pressure difference across the rotor by using Eq. (9). The extracted equation for pressure difference across the rotor is a function of upstream velocity (U_∞) and wake velocity (U_w) as shown by Eq. (10).

$$\triangle p = -\rho \Omega v_R R \qquad \textbf{(9)}$$

$$\triangle p = \frac{1}{2}\rho (U_\infty^2 - U_w^2) \qquad \textbf{(10)}$$

Fig. 16 shows the variations of power coefficient with the tip speed ratio. Results are made with and without wake rotation effect. The figure demonstrates that the wake rotation effect is well pronounced at lower value of tip speed ratio.
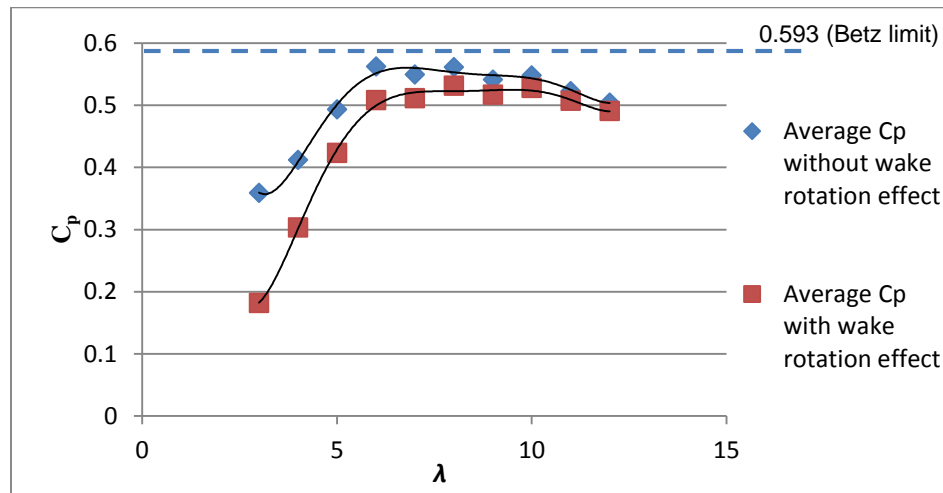
Fig. 16: *Variation of average power coefficient (Cp) along the blade with tip speed ratio (λ)*

The results are similar to those by [19] and confirm the results of axial and tangential induction factors. The power coefficient (C_p) is reduced by the wake rotation. At λ=3 reduction is 50% but the reduction decreases at higher λ to be 7.2% at λ=7 and about 2% at λ=12 as shown in the figure.

5. Conclusions

- PIV is proved to be an excellent tool to provide full map of mean velocities, turbulence intensity and vortices behind the wind turbine model.

- The wake width and length increase as λ increases up to $\lambda=9$, the wake width remains constant for higher values of λ. It should be noted that the increase of λ is directly an increase of Re_c. As Re_c increases with constant λ the velocity deficit behind the rotor increases, the wake width and length increase and turbulence intensity also increases. This conclusion is supported by the results of a previous research [12]. Turbulence intensity in the wake increases as λ increases. The increase of turbulence intensity can be accounted for the increase of Reynolds number.

- Tip speed ratio has significant effect on the tip vortices pitch. As λ increases the pitch (h) decreases and the tip vortex intensity increases. Reynolds number has a significant effect on the tip vortices intensity. Tip vortices intensity increases by the increase of Reynolds number at constant λ while the pitch is weakly affected by Re_c variation.

- Axial induction factors are generally increased by the increase of λ. At λ between 6 and 8, the induction factor has almost constant value near 0.3 (Betz limit is at a= 0.333) up to 80 % of the rotor radius then it drops to reach around 0.12 for larger radii. The tangential induction factors are also calculated by information of the tip vortices intensity to show the effect of wake rotation. The present study concludes that such range of λ between 6 and 8 is considered optimum for the turbine geometry used.

- The wake rotation also affects the value of power coefficient (C_p). Results show that power coefficient (C_p) is reduced by the wake rotation at lower λ ($\lambda=3$) by about 50%. The reduction decreases at higher λ to be about 7.2% at $\lambda=7$ and 2% at $\lambda=12$.

6. References

[1] Whale, J., Anderson, C. G., Bareiss, R. and Wagner, S., *An Experimental and Numerical Study of the Vortex Structure in the Wake of a Wind Turbine*, Wind Engineering and Industrial Aerodynamics, Vol. 84, pp. 1-21, 2000.

[2] Montgomerie, B., *The need for more Measurements*, Proceeding 4th Int. Energy Agency (IEA) Aerodynamics Symposium, Rome, Italy, 1990.

[3] Akon, A. F., Samner, D. and Trovi, D., *Measurement of Axial Induction Factor for a Model Wind Turbine*, M. Sc Thesis, Department of Mechanical Engineering, University of Saskatchewan, 2012.

[4] Vermeer, L. J., Sørensen, J. N. and Crespo, A., *Wind Turbine Wake Aerodynamics*, Progress in Aerospace Sciences,Vol. 39, PP. 467-510, 2003.

[5] Haans, W., Sant, T., Kuik, G. V. and Bussel, G. V., *HAWT Near-Wake Aerodynamics, Part I: Axial Flow Conditions*, Wind Energy, Vol. 11, PP. 245-264, 2008.

[6] Dan-mei, H. and Zhao-hui, D., *Near Wake of a Model Horizontal Axis Wind Turbine*, Journal of Hydrodynamics Vol. 21, PP. 285-291, 2009.

[7] Infield, D. G., Grant, I., Smith, G. and Wang, X., *Development of Particle Image Velocimetry for Rotor Flow Measurements*, Proceeding British Wind Energy conference, PP. 73-78, 1994.

[8] Whale, J., Papadopoulos, H., Anderson, C. G., Helmis, C. G. and Skyner D. J., *A Study of the Near Wake Structure of a Wind Turbine Comapring Measurements from Laboratory and Full-Scale Experiments*, Solar Energy, Vol. 56, PP. 621-633, 1996.

[9] XIAO, J. P., WU, J., CHEN, L. and SHI, Z. Y., *Particle Image Velocimetry (PIV) Measurements of Tip Vortex Wake Structure of Wind Turbine*, Applied Mathematics and Mechanics, Vol. 32, PP. 729-738, 2011.

[10] Yang, Z., Sarkar, P. and Hu, H., *An Experimental Investigation on the Wake Characteristics of a Wind Turbine in an Atmospheric Boundary Layer Wind*, Applied Aerodynamics Conference, Honolulu, 2011.

[11] Sherry, M., Sheridan, J. and Jacono, D. L., *Characterisation of a Horizontal Axis Wind Turbine's Tip and Root Vortices*, Experimental Fluids, Vol. 54, PP. 1417-1436, 2013.

[12] McTavish, S., Fsezty, D. and Nitzsche, F., *Evaluating Reynolds Number Effects in Small-Scale Wind Turbine Experiments*, Wind Energy and Industrial Aerodyanmics,Vol. 120, PP. 81-90, 2013.

[13] Varshney, K., *Characteristics of Helical Tip Vortices in a Wind Turbine Near Wake*, Theory Application Climatol,Vol. 111, PP. 427-435, 2011.

[14] Burton, T., Sharpe, D., Jenkins, N. and Bossanyi, E., *Wind Energy Handbook*, PP. 1-643, 2001.

[15] Zhang, W., Markfort, C. D. and Porte'-Agel, F., *Near-Wake Flow Structure Downwind of a Wind Turbine in a Turbulent Boundary Layer*, Experimental Fluids, Vol. 52, PP. 1219-1235, 2012.

[16] Ramesh, K., Ke, J., Gopalarathnam, A. and Edwards, J. R., *Effect of Airfoil Shape and Reynolds Number on Leading Edge Vortex Shedding in Unsteady Flows*, Applied Aerodynamics Conference, New Orleans, American Institute of Aeronautics and Astronautics, 2012.

[17] Sanderse, B., *Aerodynamics of Wind Turbine Wakes*, Energy Research Centre of the Netherlands, 2009.

[18] Medici, D., *Experimental Studies of Wind Turbine Wakes-Power Optimization and Wake Meandering*, KYH Mechanics, Royal Institute of technology, Stockholm, 2005.

[19] Schubel, P. and Crossley, R., *Wind Turbine Blade Design*, Energies, Vol. 5, PP. 3425-3449, 2012.